The Cryosphere Discuss., 4, 183–206, 2010
www.the-cryosphere-discuss.net/4/183/2010/

The Cryosphere
Discussions

This discussion paper is/has been under review for the journal The Cryosphere (TC).
Please refer to the corresponding final paper in TC if available.

An algorithm to detect sea ice leads using AMSR-E passive microwave imagery

J. Röhrs and L. Kaleschke

Institute of Oceanography, University of Hamburg, Bundesstraße 53, 20146 Hamburg, Germany

Received: 19 January 2010 – Accepted: 18 February 2010 – Published: 22 February 2010

Correspondence to: L. Kaleschke (lars.kaleschke@zmaw.de)

Published by Copernicus Publications on behalf of the European Geosciences Union.

Abstract

Leads are major sites of energy fluxes and brine releases at the air-ocean interface of sea ice covered oceans. This study presents an algorithm to detect leads that are broader than 3 km in the entire Arctic Ocean. The algorithm detected 50% of the lead area that is visible in optical satellite images. Passive microwave imagery from the Advanced Microwave Scanning Radiometer – Earth Observation System (AMSR-E) is used, allowing daily observations that are independent of daylight or cloud conditions. Using unique signatures of thin ice in the brightness temperature ratio between the 89 GHz and 19 GHz channels, the algorithm allowed to detect thin ice features in the ice cover and is optimized to detect leads. Leads were mapped for the period from 2002–2009 excluding the summer months. Several frequently reoccurring large scale lead patterns were found, especially in regions where sea ice is known to drift out of the Arctic Ocean. The maximum lead occurrence in the Arctic is located in the Beaufort Sea, low lead occurrence was found in the inner Arctic Ocean close to the North Pole.

1 Introduction

The Arctic sea ice cover is fractured by leads and polynyas in zones of divergence and shear motion. Although the area of these openings is relatively small during winter they are of major importance for the heat balance. The heat fluxes between open water and the atmosphere are orders of magnitudes larger than through thicker ice (Maykut, 1987). Not only leads of open water but also refrozen leads that are covered with thin ice contribute to these strong heat fluxes. According to a modelling study of (Lüpkes et al., 2008) a change of the lead fraction by 1% could cause a near-surface air temperature signal of up to 3.5 K under clear-sky conditions during polar night.

A very significant positive trend in Arctic sea ice velocity was recently reported (Hakkinen et al., 2008). A more dynamic sea ice cover exhibits more leads and openings with implications for the heat balance and the winter SAT. However, the distribu-

tion, variability and possible trends of openings in the Arctic sea ice cover are not well known.

Traditional passive microwave ice concentration data over the high concentration Arctic sea ice exhibit errors and biases that are about one magnitude larger than the true variability (Andersen et al., 2007). Thus, the existing sea ice concentration products are not suitable to study the question if the recent SAT warming in the Arctic is an early response of the system to green house gas loading (Serreze and Francis, 2006). The existing passive microwave ice concentrations (Andersen et al., 2007) show no differences between thin ice and thick multiyear ice. Measurements of the sea ice thickness and the thin ice distribution are ultimately needed for a better representation of the Arctic amplification in climate models.

Mechanisms at the air-ocean interface in the Arctic, such as heat fluxes over the sea ice, have a pronounced influence on the entire climate system (Serreze et al., 2009). Taking leads and their effects into account for boundary layer processes is therefore crucial to model weather and climate. Leads are also hypothesized as sources of atmospheric sea salt from frost flowers growing on leads (Kaleschke et al., 2004).

Leads develop as elongated cracks of open water in the ice cover. These regions refreeze as they are subject to severe cooling by the atmosphere. At first, loose ice crystals gather at the water surface (new ice or grease ice). Formation of nilas occurs if no waves are present at the freezing water surface. Nilas is a elastic thin ice cover up to 10 cm thickness of crystals that are frozen together. If waves disrupt the formation of an even thin ice cover, pancake ice forms. New Ice, nilas and pancake ice are denominated as thin ice in accordance to the World Meteorological Organization definition (WMO, 1989).

Wensnahan et al. (1993) performed a principal component analysis of thin ice microwave emission spectra and concluded that thin ice is detectable by passive microwave data, but that the information provided by passive microwave imagery does not allow to distinguish mixtures of thin ice and first year ice from each other due to the sparse ground resolution.

Cavalieri (1994) presents a microwave technique to map thin ice. This technique uses polarization ratios of the 19.4 GHz channel and differences between vertically polarized radiance components at 19.4 GHz and 37.0 GHz channels. Large areas of new ice, young ice and first year ice are distinguished this way, but the algorithm is limited to seasonal sea ice zones because thin ice and multiyear ice can not be distinguished by the used channels. Unlike to these previous studies, this work focuses on a detection of leads covered by thin ice by using the 89 GHz channel of AMSR-E.

A 5 year lead climatology for the Arctic Ocean was constructed by Miles and Barry (1998) using optical satellite images, where leads were mapped manually. Lindsay and Rothrock (1995) performed an automatic detection of leads using optical satellite imagery. These methods using optical satellite imagery allowed to recognize small leads, but are not functional during the dark season because visible channels are necessary to identify clouds. Kwok (2002) used synthetic aperture radar (SAR) derived ice motion data to retrieve openings in the ice cover. By comparing the results with passive microwave ice concentration data, Kwok showed that the ice concentrations do not account for openings in the high concentration ice cover.

A method to reveal thin ice with passive microwave imagery is presented here. The algorithm focuses on the detection of leads. We exclude large areas of thin ice as polynyas and seasonal thin ice covers, which can be detected by other techniques (Cavalieri, 1994; Markus and Burns, 1995; Kern et al., 2005). The used data and processing methods are described in Sect. 2. A way to distinguish thin ice from thicker ice in passive microwave imagery is introduced as well as a method to extract leads from the images. In Sect. 3, the results are examined and validated. A lead climatology for the Arctic is generated using the computed data.

2 Methods

2.1 Passive microwave data

Passive microwave data from JAXA's AMSR-E sensor on the NASA's Earth Observation System Aqua satellite are used to detect leads in sea ice. The AMSR-E sensor measures microwave radiation (brightness temperatures T_B) from the earth at six different frequencies while horizontally and vertically polarized radiation is measured separately for each frequency ranging from 6.9 GHz to 89.0 GHz.

The National Snow and Ice Data Center (NSIDC) provides daily averages of brightness temperatures (T_B) from the AMSR-E sensor on polar stereographic grids since summer 2002. Vertically polarized brightness temperatures at 18.7 GHz and 89.0 GHz are used in this study, specifications of these are given in Table 1.

In order to have both brightness temperatures on the same grid, $T_{B\ 18.7\mathrm{GHz}}$ is interpolated onto the 6.25 km grid. This study focuses on the detection of leads in the high concentration sea ice cover. The ARTIST Sea Ice (ASI) algorithm uses near 90 GHz channels to retrieve ice concentrations (Kaleschke et al., 2001; Spreen et al., 2008). In this study, ASI ice concentrations are used to distinguish high ice concentration areas from open water.

2.2 Thin ice in passive microwave imagery

Eppler et al. (1992) compiled microwave emissivities from different measurements for different sea ice classes in the frequencies that are typically obtained from spaceborn satellites. An assortment of those emissivities are visualized in Fig. 1, where the dashed line characterizes an emissivity ratio $r_\epsilon = 1$ with

$$r_\epsilon = \frac{\epsilon_{19V}}{\epsilon_{89V}} \tag{1}$$

ϵ_{19V} and ϵ_{89V} are the emissivities of sea ice at the vertically polarized frequencies 18.7 GHz and 89.0 GHz, respectively. It shows that only water and thin ice, meaning

new ice, nilas and pancake ice, exhibits emissivity ratios above 1, giving the possibility to distinguish thin ice from other ice types. However, light nilas, the thickest thin ice class, remains difficult to distinguish from thicker ice classes by using r_ϵ. A method to detect light nilas by using ϵ_{89V} alone was presented in Jacobi et al. (2006). Summer surface melting is in general problematic for passive microwave sea ice retrievals. Melted surfaces appear with an emissivity ratio of close to one.

The retrieval of surface emissivities from passive microwave imagery requires to model radiation transfer in the atmosphere. In order to be independent of surface and atmosphere temperature, r_ϵ will be represented by a brightness temperature ratio r. For microwave radiation, a brightness temperature $T_{B,v}$ at the frequency v can be expressed by the earth's surface temperature T_s and it's emissivity ϵ_v:

$$T_{B,v} = \epsilon_v T_s \tag{2}$$

Using Eq. (2), the emissivity ratio r_ϵ can be substituted by a brightness temperature ratio r because the influence of the unknown surface temperature is reduced:

$$r_\epsilon = \frac{\epsilon_{19V}}{\epsilon_{89V}} \simeq \frac{T_{B,19V}}{T_s} \cdot \frac{T_s}{T_{B,89V}} = \frac{T_{B,19V}}{T_{B,89V}} = r \tag{3}$$

As shown in Fig. 1, r_ϵ enables to distinguish between thin ice and thicker ice. An example of r, as defined in Eq. (3), is shown in Fig. 2 for the central Arctic. As expected from Fig. 1, regions of open water, coastal polynyas and large leads are characterized by $r > 1$.

2.3 Spatial filtering

A closer examination of Fig. 2 shows that presumptive leads, linear features in the ice cover, do not always have r values above one. The profile (Fig. 2b) at the red line in Fig. 2a crosses four leads and shows that r at the leads is just above 0.88 even though the physically expected value is $r > 1$. The large footprint of the AMSR-E sensors (compare Table 1) causes a signal of a narrow lead to appear as a mixture between a

lead signal and a thick ice signal. Therefore leads, that are narrower than the sensors footprint, can not be characterized by their r value solely but rather by their appearance as r anomalies (r'). More precisely, leads are regions with high r values surrounded by lower r values of thick ice. This may be expressed by the relation $r = \overline{r} + r'$. A high pass filter is implemented to retrieve r':

$$r' = r - \text{Median}_w(r) \tag{4}$$

A median filter is used to represent $\overline{r}$ because it has proven to detect leads better than linear shift invariant (LSI) filters. It removes anomalies such as leads but preserves edges between large constant areas. A LSI edge detection filter did not exclusively deliver lead regions but also edges between other thick ice classes, ice edges to open water and edges to large atmospheric disturbances.

The median operator in Eq. (4) replaces the center pixel of a search window with the median value of all pixels within the search window. The size of the search window is $w \times w$ pixel. The parameter w needs to be optimized for sensor characteristics.

2.4 Definition of a thin ice concentration

Leads are recognized by their thin ice cover. A thin ice concentration (TIC) is defined analogously to the sea ice concentration to describe the area fraction of thin ice compared to other ice classes. The TIC is defined as follows: An upper tiepoint r'_{100} of the r' value sets a TIC of 100% and a lower tiepoint r'_0 sets a TIC of 0%. In between the two tiepoints, the TIC is interpolated linearly.

$$\text{TIC} = \begin{cases} 1 & \text{if } r' > r'_{100} \\ 0 & \text{if } r' < r'_0 \\ \frac{r' - r'_0}{r'_{100} - r'_0} & \text{if else} \end{cases} \tag{5}$$

In order to focus on leads in the closed ice cover, pixel that contain more than 10% open water according to ASI ice concentration are not considered. The threshold of

10% is chosen to blend out the ice edge. However, pixel which have r values that correspond to open water are not sorted out by the algorithm. Therefore, open water regions that are not classified as open water according to ASI ice concentrations are assigned with high TIC.

2.5 MODIS data

All parameters, the window size w of the median filter and the upper and lower tiepoints for the TIC definition, are obtained by comparing the respective results of TICs with visible satellite images. In visible satellite images, open water and thin ice appear as dark regions (low reflectance). For cloud free daylight conditions, the high resolution of visible satellite images enables a reliable identification of leads.

The Moderate Resolution Imaging Spectroradiometer (MODIS) aboard the Aqua EOS and Terra EOS satellites acquires data in 36 different spectral bands. Band 3 of the MODIS sensor (459 nm–479 nm) has a spatial resolution of 500 m and is used to determine the above mentioned parameters and for validation of the TIC product. In order to evaluate if the computed TICs do indeed mark thin ice regions, TICs are overlaid onto MODIS band 3 images.

3 Results

3.1 Adjustment of algorithm parameters

The search window size w in Eq. (4) is optimized to detect leads. A too small search window does not detect broad leads while a too large search window disturbs small scale lead signals if several leads are close together. Comparing results of different w showed satisfying results for values of 5, 7 and 9 pixel. Therefore $w = 7$ is used, corresponding to an area of 44 km × 44 km.

Figure 3 shows a frequency distribution of r' values for thin ice pixels and for pixels that do not contain thin ice. Here, visible satellite imagery is used to determine if a

pixel contains thin ice or not. Thin is is classified by a reflectance lower than 0.65 in band 3 of the MODIS sensor. In Fig. 3, values of $r' \gtrsim 0.05$ are only present for thin ice, indicating that the area represented by those pixels only contains thin ice. $r' = 0.05$ is therefore used as a first guess tiepoint for 100% thin ice concentration.

The validation in Sect. 3.3 shows that the first guess upper tiepoint gives generally reasonable results. The validation also shows that $r' = 0.015$ is a lower tiepoint that enables the detection of even small leads while keeping noise on a low level.

3.2 Thin ice distribution patterns

Daily thin ice concentrations (TICs) for the northern hemisphere are calculated from September 2002 until December 2009 excluding the summer months June, July and August, where the algorithm is not applicable. Exemplary TIC maps are shown in Fig. 4.

The following features dominate the TIC maps: A) linear features of high TIC (leads) are present in most of the TIC maps. Leads often appear between the North Pole and the Fram Strait, as in Fig. 4a, b, d, and north of the Canadian Archipelago and Greenland (Fig. 4a, b, c). B) Irregular structures of TIC are very often present in the Beaufort Sea. C) Coastal polynyas are often visible at the Canadian Archipelago, in the Laptev Sea and in the East Siberian Sea.

Looking at series of subsequent TIC maps, the following impression appears: D) leads remain present several days after their appearance, are strong subject to the ice movement and deformation and disappear suddenly (from one day to another). E) The irregular structures of TIC in the Beaufort Sea usually underlies the rotation of the Beaufort Gyre which is described by (Rigor et al., 2002). F) Coastal polynyas are stationary features and remain present for more than a few days.

Some specific lead patterns, which reoccurred frequently from September 2002 until December 2009, are found in the TIC maps: G) parallel circle segments of leads that are located stream upwards of outflow passages of sea ice from the Arctic Ocean. This pattern frequently occurred north of the Fram Strait, as visible in Fig. 4a, d. On

a smaller scale, this pattern frequently occurred north of the Nares Strait, which is located between the northern edge of Greenland and Ellesmere Island (Fig. 4c). H) The frequently occurring coastal polynyas at the Canadian Archipelago tend to be extended by larger leads, pointing away from land. These leads are orientated towards north or north-east (Fig. 4b).

3.3 Validation of thin ice concentrations

In this investigation, the detection of leads are considered as the primary usage of the TIC maps. Therefore, the validation of TIC focuses on linear structures of thin ice (presumptive leads).

Figure 5 shows scenes from the Beaufort Sea during different seasons. Banks Island is located in the lower left corner of all three images, some parts of the Queen Elisabeth Island are located in the lower right corner. Note that a validation using visible satellite imagery is not possible during the dark season in the Arctic (November until February) because daylight is required.

Figure 5a shows a scene at the 21 March 2006. Broad leads are overlapped with high TIC and some of the narrow leads are covered by low TIC. The most narrow leads are not detected. A few pixels of low TIC are present where no thin ice or water is visible in the optical image, for instance in the upper right quadrant of Fig. 5a. These pixels must be regarded as failures of the lead detection. A polynya at Banks Island can be seen in Fig. 5a, where the TIC is low in some parts of the polynya. This will be discussed in Sect. 4.

Figure 5b, c show similar relations between optical images and TICs as Fig. 5a. An autumn scene (25 September 2007) from the same region as in Fig. 5a is shown in Fig. 5b. Here, the ice edge is located in the image. Many leads are visible in the optical image, most of them appear in a pattern of parallel circle segments. This pattern is identifiable in the TIC as well.

Figure 5c shows a scene at the 3 May 2007. Here, Ellesmere Island is located in the lower right corner. Large leads are recognized by the thin ice detection while the

polynya near Banks Island is not marked as thin ice (Compare Fig. 5a).

These results were obtained with the parameters given in Sect. 3.1. The linear structures of high TIC, that were found in Fig. 4 and described in Sect. 3.2, can indeed be identified as leads. The width of the smallest leads that are certainly detected can be identified as 3 km. This number is determined by measuring the width of the leads in Fig. 5a manually. In this scene, all leads with a width larger than 3 km were marked by a TIC larger than 5%. Smaller leads are detected occasionally.

Each TIC pixel in Fig. 5a, c was evaluated independently of its r' value whether it contains thin ice or not using the corresponding MODIS image as described in Sect. 3.1. This information was used to obtain a frequency distribution of the r' values from thin ice pixel (Fig. 3). All pixel with r' values above the lower tiepoint r'_0 (left red line) were classified as thin ice by the lead detection algorithm. The shaded area underneath the thin ice curve in Fig. 3 represents thin ice containing pixel that were identified as thin ice pixel by the lead detection. The area underneath the entire thin ice curve represents the number of pixel that contain leads according to the MODIS image. The ratio between these areas gives an estimate of how much thin ice containing pixel were found by the lead detection compared to how many pixel are identifiable as thin ice pixel in the MODIS image. In the investigated scene, about 50% of the thin ice containing pixel were detected by the lead detection algorithm.

3.4 A lead climatology

An mean TIC from September 2002 to December 2009 is shown in Fig. 6. It is remarked that only smaller thin ice occurrences (such as leads) are detected while large areas of thin ice are not captured. Pixels with ASI ice concentrations below 90% are not included in the averaging of TIC.

High lead activity is present in the Beaufort Sea, with a maximum close to Banks Island. The shape of this thin ice region suggests a strong connection with the ice drift in the Beaufort Gyre, described by Rigor et al. (2002). In the inner Arctic Ocean, close to the north pole, the averaged thin ice concentrations are below 2%. A considerable

higher lead activity is located in the Fram Strait and in the region stream upwards of the Fram Strait. A rather small region north of the Nares Strait shows high average TICs above 20%. In coastal regions, high thin ice concentrations are present. These represent either frequently occurring coastal polynyas or are an artifact of the microwave image sensor footprint which is regarded in Sect. 4.

4 Discussion

A way to distinguish thin ice from other ice types using microwave imagery is presented. Two different frequencies from the AMSR-E sensor are combined to one product, a T_B ratio in which thin ice theoretically has significant values above 1. The combination of data in these two different frequencies involves different sensor footprints. Therefore, the combined product of these frequencies does not represent the real microwave emission characteristics of sea ice. Also, the T_B ratio signal of one pixel might originate from different sea ice classes that are present in the footprint area. Due to these two reasons, thin ice on small leads has not the physical expected T_B ratio and can thus not be identified by the T_B ratio. Spatial anomalies of the T_B ratio are used instead to detect thin ice. This technique enables a detection of leads that are larger than 3 km, which is below the resolution of the used microwave imagery. The high radiometric contrast between thin ice and thicker ice and the additional information that leads are narrow is used to obtain this result using a high pass filter.

The lead detection algorithm presented here does not detect large areas of thin ice. For example, coastal polynyas can be seen in Fig. 5a, c. At the broadest part of the polynya in Fig. 5a, the TIC decreases to low values. The large polynya in Fig. 5c is marked with zero TIC. At narrow parts of the polynyas, the TIC has reasonable high values. The fact, that the TIC algorithm does not detect large regions of thin ice, arises because the algorithm uses a spatial high pass filter. It enables a detection of subpixel scale leads but causes the algorithm not to detect larger thin ice areas. The lead detection presented here is optimized to detect narrow leads. Other techniques exist

to recognize large areas of thin ice and polynyas (Cavalieri, 1994; Markus and Burns, 1995; Kern et al., 2005). The T_B ratio of the 89.0 GHz and 18.7 GHz channels, which is used here, could also be used to detect large areas of thin ice if the spacial filter would not be implemented.

Wensnahan et al. (1993) concluded that smaller areas of thin ice can not be detected by passive microwave imagery due to their low resolution. The technique presented in this study utilizes the 89 GHz channel of the AMSR-E sensor with a considerable higher resolution than other microwave channels. Together with the spatial filter, this channel enables to distinguish even subpixel scale occurrences of thin ice from other ice classes. In particular, leads covered by thin ice can be detected by the presented technique. Optical satellite images showed that leads with a width of 3 km or larger are detected fairly well. 50% of the lead area in MODIS images are identified as lead pixel by the passive microwave algorithm.

Figures 4 and 6 show high thin ice concentrations at coasts that represent polynyas but could also originate from land microwave emissions. A technique to reduce the effect of coasts on microwave imagery is developed by Maaß and Kaleschke (2009). However, the validation of TICs with MODIS images showed coastal polynyas in the examined scenes.

The presented lead detection is applicable when AMSR-E passive microwave imagery with the high resolution 89 GHz channel is available. This includes the entire Arctic and Antarctic on a daily basis. No daylight is required and clouds cause no serious limitation. The lead detection is not applicable during the summer months (June, July, August) when surface melting modifies the ice emissivity. This becomes obvious when looking at the emissivities of the summer melting ice class in Fig. 1, where summer melting has a similar emissivity ratio as nilas. Also does high atmospheric moisture during summer affect the signal of the 89 GHz channel.

Earlier lead detection studies used optical or SAR data to locate leads (Miles and Barry, 1998; Kwok, 2002). The high resolution of optical and SAR data reveals leads that are orders of magnitudes smaller than the leads detected in this study. However,

the new lead detection using passive microwave data enables an investigation of leads with a better temporal coverage. In further studies, the new lead detection could be used to investigate the dynamical processes that cause the formation of leads.

The average TIC from 2002 until 2009 (Fig. 6) highlights areas where leads often occurred. A region with considerable high lead occurrence is the Beaufort Sea, which is in accordance to the results of Miles and Barry (1998). Rigor et al. (2002) described the ice drift in the Beaufort Sea, it follows the rotational movement of the Beaufort Gyre. Rigor et al. (2002) explain that the anticyclonic motion in the atmosphere causes divergent Ekman transport at the sea surface, leading to the formation of leads and thinning of sea ice. This explains the high average TIC in the Beaufort Sea. Accordingly, regions of low ice deformation also show low average TIC, i.e. the inner Arctic Ocean where the less deformational transpolar ice drift is located (Rigor et al., 2002).

Other regions with high TICs were stream upwards of outflow passages of sea ice from the Arctic Ocean, as the Fram Strait and the Nares Strait. In these two regions, parallel circle segments of leads are often present. These parallel circle segments, also refered as arches, form as a consequence to the outflow of ice through lateral boundaries on both sides. The formation of arch-shaped leads due to displacement restrictions at the region boundaries has been described by Goldstein et al. (2000). Kwok et al. (2010) investigated the ice outflow through the Nares Strait using SAR images and concluded that the arches of ice slow down the ice export through the passage because of their structural strenght.

Total ice concentrations are often used to estimate heat fluxes from the ocean. Thin ice and thick multiyear ice are not distinguished in passive microwave ice concentrations, leads covered by thin ice should therefore show 100% ice concentration (Andersen et al., 2007). In this study, regions with ASI ice concentrations below 90% are excluded. Therefore, all detected leads coincide with higher total ice concentrations. The here defined thin ice concentration could therefore serve as a useful additional tool beside total ice concentration to describe the surface properties of sea ice covered oceans. Especially if surface energy fluxes are to be estimated, the total ice concen-

tration does not represent the diverse conditions of thin ice and thicker ice.

5 Conclusions

Based on microwave emission properties of sea ice, a method to detect sea ice leads is presented. Thin ice has a unique signature in the ratio of the brightness temperatures at 89 GHz and 19 GHz. The algorithm allows the detection of thin ice covered leads, open water leads and polynyas that are broader than 3 km. 50% of the total lead area that is visible in 500 m resolution optical satellite images is detected by the algorithm. The leads that are detected coincide with high total ice concentrations. The new thin ice product does therefore deliver additional information to describe the surface properties of the Arctic Ocean, especially if heat fluxes shall be estimated.

During 2002 until 2009, leads or other thin ice features are located mainly in the Beaufort Sea and close to the Fram Strait, where average TICs were up to 20%. The inner Arctic Ocean close to the north pole shows low lead occurrence with average TICs below 2%. Smaller areas of high average TICs were found stream upwards of the Nares Strait and close to coasts, where coastal polynyas are often present.

Frequently reoccurring patterns of leads were identified, i.e. parallel circle segments of leads stream upwards of the Fram Strait and the Nares Strait or leads that are extensions of coastal polynyas. The detected leads had a life time of several days and were strong subject to ice drift and deformation, especially in the rotational movement in the Beaufort Sea.

Acknowledgements. This work has been funded by the German Science Foundation (DFG) via SFB512, Teilprojekt E5.

References

Andersen, S., Tonboe, R., Kaleschke, L., Heygster, G., and Pedersen, L.: Intercomparison of passive microwave sea ice concentration retrievals over the high-concentration Arctic sea

ice, J. Geophys. Res, 112, C08004, doi:10.1029/2006JC003543, 2007. 185, 196

Cavalieri, D.: A microwave technique for mapping thin sea ice, J. Geophys. Res.-Oceans, 99, 12561–12572, 1994. 185, 186, 195

Eppler, D., Farmer, L., Lohanick, A., Anderson, M., Cavalieri, D., Comiso, J., Gloersen, P., Garrity, C., Grenfell, T., Hallikainen, M., Maslanik, J., Mätzler, C., Melloh, R., Rubinstein, I., and Swift, C.: Passive microwave signatures of sea ice, in: Microwave Remote Sensing of Sea Ice, edited by Carsey, F. D., no. 68 in Geophysical Monograph, American Geophysical Union, 1992. 187, 201

Goldstein, R. V., Osipenko, N. M., and Leppäranta, M.: Classification of Large-Scale Sea-Ice Structures Based on Remote Sensing Imagery, Geophysica, 36, 95–109, 2000. 196

Hakkinen, S., Proshutinsky, A., and Ashik, I.: Sea ice drift in the Arctic since the 1950s, Geophys. Res. Lett., 35, L19704, doi:10.1029/2008GL034791, 2008. 184

Jacobi, H., Kaleschke, L., Richter, A., Rozanov, A., and Burrows, J.: Observation of a fast ozone loss in the marginal ice zone of the Arctic Ocean, J. Geophys. Res.-Atmos., 111, D15309, doi:10.1029/2005JD006715, 2006. 188

Kaleschke, L., Heygster, G., Lüpkes, C., Bochert, A., Hartmann, J., Haarpaintner, J., and Vihma, T.: SSM/I sea ice remote sensing for mesoscale ocean-atmosphere interaction analysis: Ice and icebergs, Can. J. Remote Sens., 27, 526–537, 2001. 187

Kaleschke, L., Richter, A., Burrows, J., Afe, O., Heygster, G., Notholt, J., Rankin, A., Roscoe, H., Hollwedel, J., Wagner, T., et al.: Frost flowers on sea ice as a source of sea salt and their influence on tropospheric halogen chemistry, Geophys. Res. Lett., 31, L16114, doi:10.1029/2004GL020655, 2004. 185

Kern, S., Harms, I., Bakan, S., and Chen, Y.: A comprehensive view of Kara Sea polynya dynamics, sea-ice compactness and export from model and remote sensing data, Geophys. Res. Lett., 32, L15501, doi:10.1029/2005GL023532, 2005. 186, 195

Kwok, R.: Sea ice concentration estimates from satellite passive microwave radiometry and openings from SAR ice motion, Geophys. Res. Lett., 29, 1311, doi:10.1029/2002GL014787, 2002. 186, 195

Kwok, R., Pedersen, L. T., Gudmandsen, P., and Pang. S. S.: Large sea ice outflow into the Nares Strait in 2007, Geophys. Res. Lett., 37, L03502, doi:10.1029/2009GL041872, 2010. 196

Lindsay, R. and Rothrock, D.: Arctic sea ice leads from advanced very high resolution radiometer images, J. Geophys. Res.-Oceans, 100, 4533–4544, 1995. 186

Lüpkes, C., Vihma, T., Birnbaum, G., and Wacker, U.: Influence of leads in sea ice on the temperature of the atmospheric boundary layer during polar night, Geophys. Res. Lett., 35, L03805, doi:10.1029/2007GL032461, 2008. 184

Maaß, N. and Kaleschke, L.: Improving passive microwave sea ice concentration algorithms for coastal areas – applications to the baltic sea, Tellus, submitted, 2009. 195

Markus, T. and Burns, B.: A method to estimate subpixel-scale coastal polynyas with satellite passive microwave data, J. Geophys. Res.-Oceans, 100, 4473–4487, 1995. 186, 195

Maykut, G.: Energy exchange over young sea ice in the central Arctic, J. Geophys. Res.-Oceans, 83, 3646–3658, 1987. 184

Miles, M. and Barry, R.: A 5-year satellite climatology of winter sea ice leads in the western Arctic, J. Geophys. Res.-Oceans, 103, 21723–21734, 1998. 186, 195, 196

Rigor, I. G., Wallace, J. M., and Colony, R. L.: Response of Sea Ice to the Arctic Oscillation, J. Climate, 15, 2648–2662, 2002. 191, 193, 196

Serreze, M. and Francis, J.: The Arctic amplification debate, Climatic Change, 76, 241–264, 2006. 185

Serreze, M. C., Barrett, A. P., Stroeve, J. C., Kindig, D. N., and Holland, M. M.: The emergence of surface-based Arctic amplification, The Cryosphere, 3, 11–19, 2009, http://www.the-cryosphere-discuss.net/3/11/2009/. 185

Spreen, G., Kaleschke, L., and Heygster, G.: Sea ice remote sensing using AMSR-E 89 GHz channels, J. Geophys. Res, 113, C02S03, doi:10.1029/2007GL032461, 2008. 187

Wensnahan, M., Maykut, G., Grenfell, T., and Winebrenner, D.: Passive microwave remote sensing of thin sea ice using principal component analysis, J. Geophys. Res.-Oceans, 98, 12453–12468, 1993. 185, 195

WMO: The World Meteorological Organization Sea-Ice Nomenclature (WMO No. 259, TP-145, Supplement No. 5), 1989. 185

Table 1. Specifications of used channels from the AMSR-E sensor.

Channel	Sensor footprint	NSIDC grid
89.0 GHz	6 km × 4 km	6.25 km
18.7 GHz	27 km × 16 km	12.5 km

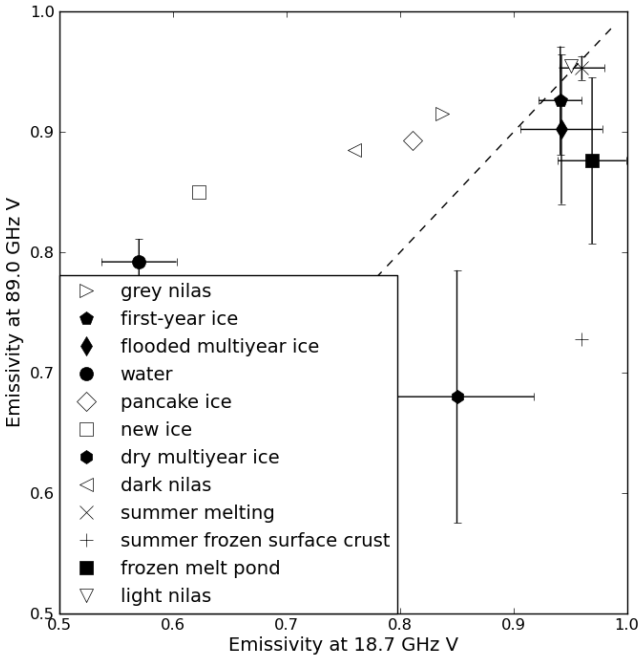

Fig. 1. Emissivities of different sea ice classes in a comparison of the vertical polarized frequencies 18.7 GHz and 89.0 GHz. Thin ice classes are plotted with contoured markers, other ice classes and open water with solid markers. The dashed line shows an emissivity ratio of $r_\epsilon = 1$. The values are taken from Eppler et al. (1992). The error bars display standard deviations if available.

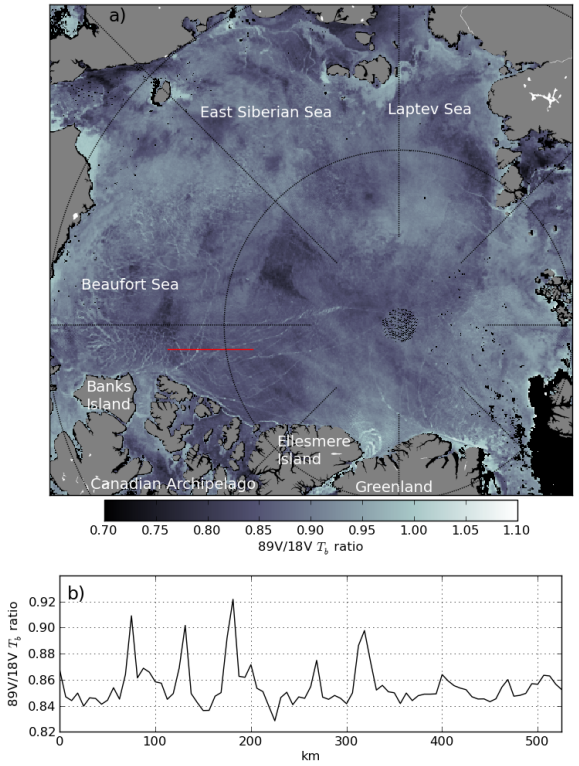

Fig. 2. **(a)** Brightness temperature ratio r of the 89.0 GHz V and 18.7 GHz V channels at the 27.02.2007. in the Arctic Ocean. **(b)** r profile at the red line.

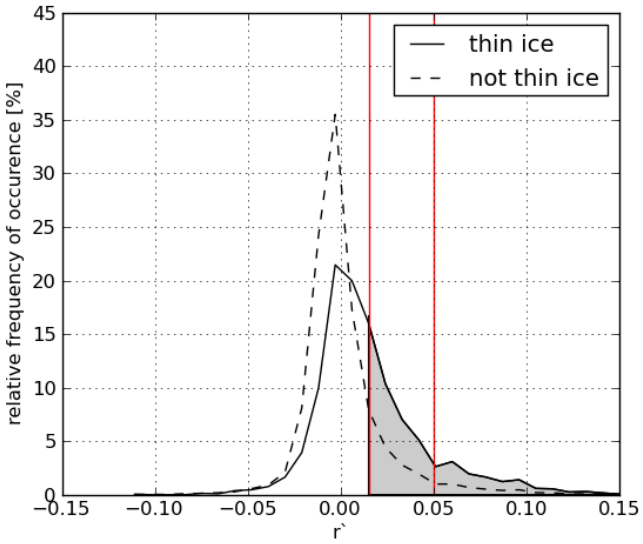

Fig. 3. Frequency distribution of r' values for the scene in Fig. 5a. The red lines mark the lower and upper tiepoints r'_0 and r'_{100} in Eq. (5).

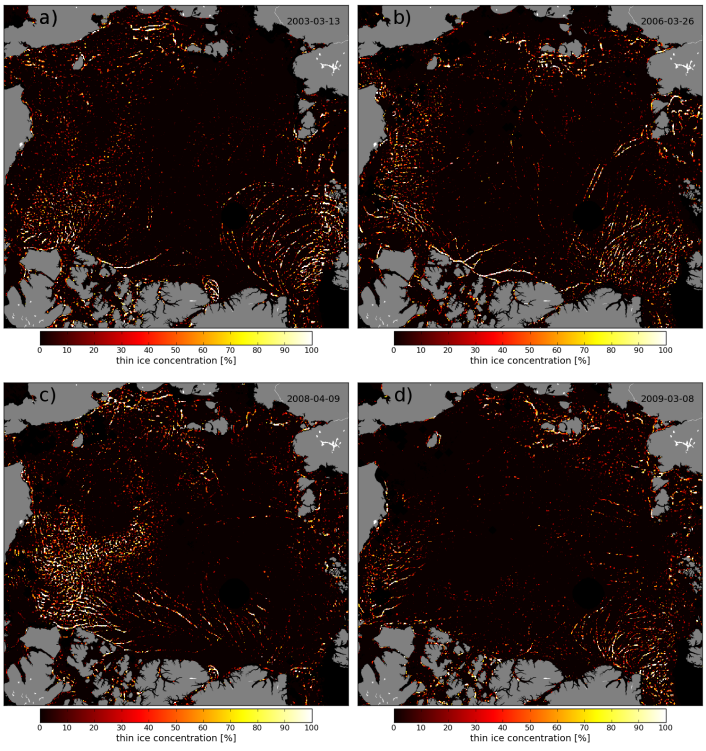

Fig. 4. Thin ice concentrations in the Arctic Ocean as defined in Sect. 2.4.

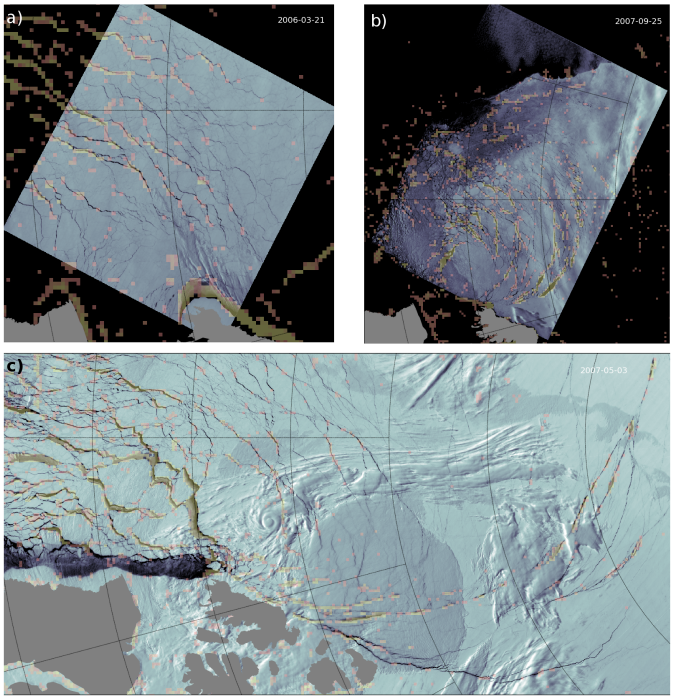

Fig. 5. Comparison of thin ice concentrations with optical satellite images (MODIS band 3). The optical images are displayed in grayscale, TICs are displayed in opaque color from reddish (5%) to yellow (100%). The TIC pixel cover an area of 6.25 km×6.25 km.

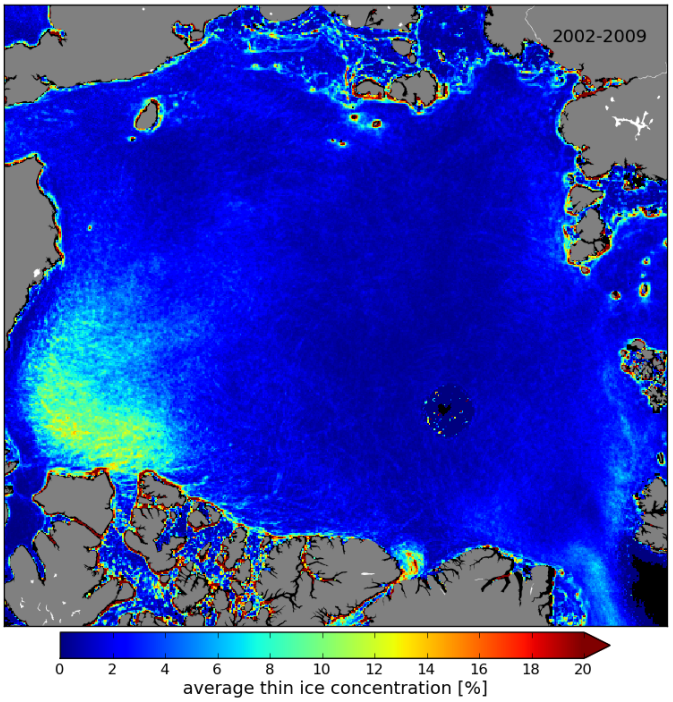

Fig. 6. Average of thin ice concentrations from 2002 to 2009 excluding the summer months June, July and August.